Research Square

Preprints are preliminary reports that have not undergone peer review.
They should not be considered conclusive, used to inform clinical practice,
or referenced by the media as validated information.

# Comparative Thermomechanical Performance of CFRP and PETG for UAV Structures under Thermal Extremes

**Juneed Yawar**

Juneedyawar@nitsri.ac.in

National Institute of Technology Srinagar

**Mohammad Mursaleen**

National Institute of Technology Srinagar

**Research Article**

**Keywords:** Unmanned Aerial Vehicle, Carbon Fiber Reinforced Polymer, Polyethylene Terephthalate Glycol, Thermomechanical properties, ASTM mechanical testing, Temperature-dependent behavior

**Posted Date:** March 30th, 2026

**DOI:** https://doi.org/10.21203/rs.3.rs-8792151/v1

**License:** This work is licensed under a Creative Commons Attribution 4.0 International License.
Read Full License

**Additional Declarations:** No competing interests reported.

**Version of Record:** A version of this preprint was published at CEAS Aeronautical Journal on September 28th, 2026. See the published version at https://doi.org/10.1007/s13272-026-01015-4.

# Comparative Thermomechanical Performance of CFRP and PETG for UAV Structures under Thermal Extremes

**Juneed Yawar*[1], Mohammad Mursaleen[2]**

[1,2] *Department of Mechanical Engineering, National Institute of Technology Srinagar, Jammu & Kashmir, India, 190006*

* *Juneedyawar@nitsri.ac.in*

**Abstract-** The selection of structurally resilient and thermally stable materials is critical in the design of unmanned aerial vehicle (UAV) frames that operate in varied environmental conditions. In this study, two candidate materials, Carbon Fiber Reinforced Polymer (CFRP) and Polyethylene Terephthalate Glycol (PETG), were systematically evaluated for their thermomechanical performance. Standardized ASTM tests were conducted on samples conditioned at −10°C, 40°C, and 55°C for 12 hours, simulating the typical operational environments experienced by UAVs. CFRP specimens were tested using ASTM D3039-17 (tensile), ASTM D7264/D7264M-21 (flexural), and ASTM D2344/D2344M-22 (short-beam shear), while PETG samples were tested using ASTM D638-14 for tensile behavior. Mechanical properties including ultimate tensile strength, flexural strength, and interlaminar shear strength were recorded and analyzed in megapascals (MPa). The results reveal that CFRP retained approximately 91.7% of its tensile strength across temperatures with minimal degradation, while PETG showed a tensile strength reduction ranging from 11.1% to 20.2%, along with a marked shift from brittle to ductile failure behavior. Fractographic analysis confirmed distinct failure patterns across temperature regimes. These findings establish a material selection benchmark and support CFRP as the preferred material for UAV structures in harsh or variable thermal environments.

**Keywords:** Unmanned Aerial Vehicle, Carbon Fiber Reinforced Polymer, Polyethylene Terephthalate Glycol, Thermomechanical properties, ASTM mechanical testing, Temperature-dependent behavior

## 1. INTRODUCTION

In the rapidly evolving aerospace and defense sectors, the demand for efficient, lightweight, and mechanically robust materials for UAVs has become increasingly critical. UAVs are now widely deployed in reconnaissance, payload delivery, surveillance, disaster relief, and

Corresponding author: Juneed Yawar, Juneedyawar@nitsri.ac.in

civilian logistics [1-7]. Their operational success is highly dependent on structural integrity, weight efficiency, and the ability to withstand thermal and mechanical stresses across a broad range of environmental conditions. Consequently, the careful selection of structural materials for UAV frames is paramount, especially when vehicles are subjected to extreme cold or high ambient temperatures during flight or ground storage [8-19].

CFRPs are widely used in the aerospace sector due to their high stiffness-to-weight ratio, low thermal expansion coefficient, and excellent fatigue resistance [20-30]. As composite materials comprising carbon fibers embedded in a thermosetting resin matrix, CFRPs provide directional strength and are tailored for high-performance structures, including UAV frames, wings, and fuselage components [31-33]. CFRPs exhibit excellent mechanical integrity even at elevated or sub-zero temperatures, making them attractive candidates for UAVs that experience temperature variations during take-off, altitude change, and mission durations [34, 35].

PETG, on the other hand, is a thermoplastic polyester commonly employed in consumer and industrial applications due to its processability, transparency, chemical resistance, and recyclability [36, 37]. In the context of UAVs, PETG is increasingly considered for low-cost frame structures, prototyping, and lightweight enclosure applications, especially in additive manufacturing [38-42]. PETG is popular for 3D-printed drone bodies and housings; however, its mechanical performance is strongly temperature-dependent. As a thermoplastic material, PETG undergoes softening and creep deformation when subjected to elevated temperatures, while becoming brittle at low temperatures. Thus, its reliability in critical UAV applications remains questionable without a thorough thermal-mechanical assessment [43-50].

Unlike previous studies that focused only on room temperature behavior or basic tensile properties, this study simulates operational UAV thermal extremes using standardized testing protocols, enabling high-fidelity material selection. The objective of this research is to comparatively evaluate the thermomechanical behavior of CFRP and PETG materials using a consistent and standardized testing framework. The materials were conditioned at −10°C (cold environments such as high-altitude flights), 40°C (ambient operational temperatures), and 55°C (hot ground conditions or direct sunlight exposure) for 12 hours prior to testing. These conditions reflect scenarios faced by UAVs in military, desert, and high-altitude applications.

Corresponding author: Juneed Yawar, Juneedyawar@nitsri.ac.in

Additionally, the study introduces a quantitative evaluation based on percentage strength retention across thermal conditions, offering a direct and comparative insight into material degradation, which has not been systematically reported in previous UAV-relevant literature.

Mechanical testing was carried out according to widely accepted ASTM protocols. CFRP was evaluated using ASTM D3039-17 for tensile strength, ASTM D7264/D7264M-21 for flexural strength, and ASTM D2344/D2344M-22 for short-beam shear strength. PETG was tested using ASTM D638-14, a standard for determining the tensile properties of plastics. These tests provided a complete profile of how both materials respond to tensile and bending loads under different thermal environments.

This work contributes to the field by providing an in-depth, data-driven assessment of these materials' suitability for UAV frame structures. It also offers practical insights into performance degradation trends, failure mechanisms, and operational safety considerations. The outcome of this study aims to aid UAV designers, aerospace engineers, and material scientists in making informed decisions regarding material selection for UAVs operating under varying thermal conditions.

## 2. EXPERIMENTAL METHODOLOGY

### *2.1 Materials*

Two distinct materials were selected for comparative thermomechanical evaluation: Carbon Fiber Reinforced Polymer and Polyethylene Terephthalate Glycol. The CFRP specimens were fabricated from commercially available, pre-cured unidirectional carbon fiber sheets bonded in a laminated matrix structure [51, 52]. These sheets were cut according to the standard dimensions prescribed by each ASTM testing protocol. PETG specimens were fabricated using Fused Deposition Modeling 3D printing to ensure uniformity and were post-processed to eliminate edge defects [49, 53, 54]. Due to the thermoplastic nature of PETG, its low modulus and poor flexural rigidity made it unsuitable for standardized flexural or interlaminar shear tests. Therefore, only tensile strength was evaluated to avoid invalid comparisons and ensure meaningful results.

### *2.2 Thermal Conditioning Protocol*

All samples were thermally conditioned before mechanical testing to simulate environmental exposure. Each specimen was subjected to three temperatures — −10°C (cold),

Corresponding author: Juneed Yawar, Juneedyawar@nitsri.ac.in

40°C (ambient), and 55°C (hot) — for a consistent duration of 12 hours in a programmable environmental chamber. These temperature ranges were selected to mimic UAV operational extremes: cold-weather reconnaissance, average room operation, and high-solar-load ground deployment. After the conditioning period, the samples were tested within 5 minutes of removal to minimize thermal rebound effects. All mechanical tests were conducted in a laboratory environment at controlled ambient room temperature ($23 \pm 2$°C) to ensure consistency across specimens.

Figure 1 shows the specimens prepared for mechanical testing after thermal conditioning at three different temperatures. In Figure 1a, the specimens are shown immediately after exposure to −10°C, representing high-altitude UAV conditions. The materials appear rigid and well-formed. Figure 1b shows specimens at 40°C, serving as the baseline ambient condition, with no visual change apparent. Figure 1c captures specimens exposed to 55°C, simulating high-temperature ground environments; PETG samples may show surface gloss or mild deformation due to heat. The images confirm uniform dimensions and surface quality across all conditions, ensuring reliable comparison in mechanical testing.

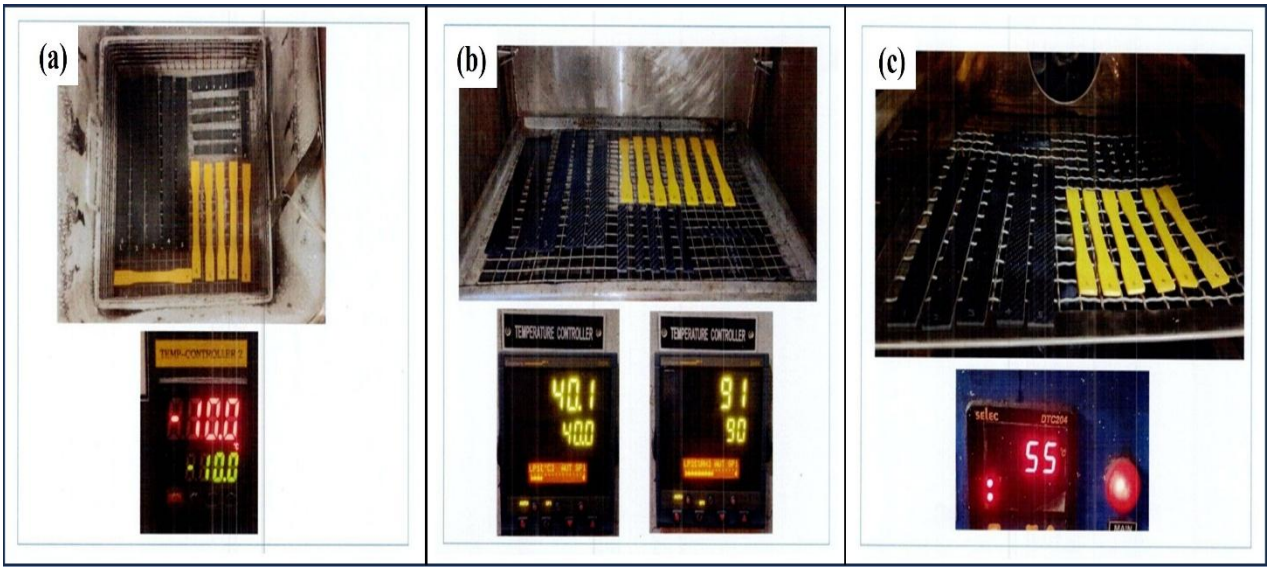



**Fig.1.** Specimens prepared for mechanical testing after 12-hour thermal conditioning at (a) −10°C, (b) 40°C, and (c) 55°C.

*2.3 Mechanical Testing Standards and Setup*

Corresponding author: Juneed Yawar, Juneedyawar@nitsri.ac.in

Testing was conducted using a fully calibrated Universal Testing Machine (UTM) with a maximum load capacity of 20 kN. The load cell and grips were configured according to the material and test type.

CFRP specimens were tested as follows:

ASTM D3039-17 – Tensile testing of polymer matrix composites

ASTM D7264/D7264M-21 – Flexural strength via 3-point bending

ASTM D2344/D2344M-22 – Interlaminar shear strength via short-beam shear method

PETG specimens were tested using:

ASTM D638-14 – Tensile strength testing for plastics

All test samples were prepared to meet the dimensional requirements of the respective ASTM standards. The tensile test speed was 2 mm/min, and for flexural tests, a crosshead rate of 1.3 mm/min was applied. Each test was conducted on three specimens per condition to ensure statistical relevance.

To quantify mechanical degradation across temperature conditions, the percentage change in strength was calculated using the following equation:

$$\%\, Drop = \frac{S_{initial} - S_{final}}{S_{initial}} \times 100$$

Where $S_{initial}$ and $S_{final}$ are the average mechanical strengths (in MPa) at −10°C and 55°C, respectively. This approach was used consistently for tensile, flexural, and shear performance comparison.

Figure 2 shows the tensile test configuration for CFRP specimens tested under ASTM D3039-17 across three thermal conditions. In Figure 2a (−10°C), the CFRP specimen is clamped in a brittle state, with the matrix likely rigid and prone to fracture. Figure 2b depicts the setup at 40°C, the standard ambient condition, where the laminate remains stable. Figure 2c shows the test at 55°C, where elevated temperatures may slightly soften the resin. In all three cases, proper axial alignment and gripping are maintained to prevent slippage or bending, ensuring accurate tensile strength evaluation.

Corresponding author: Juneed Yawar, Juneedyawar@nitsri.ac.in

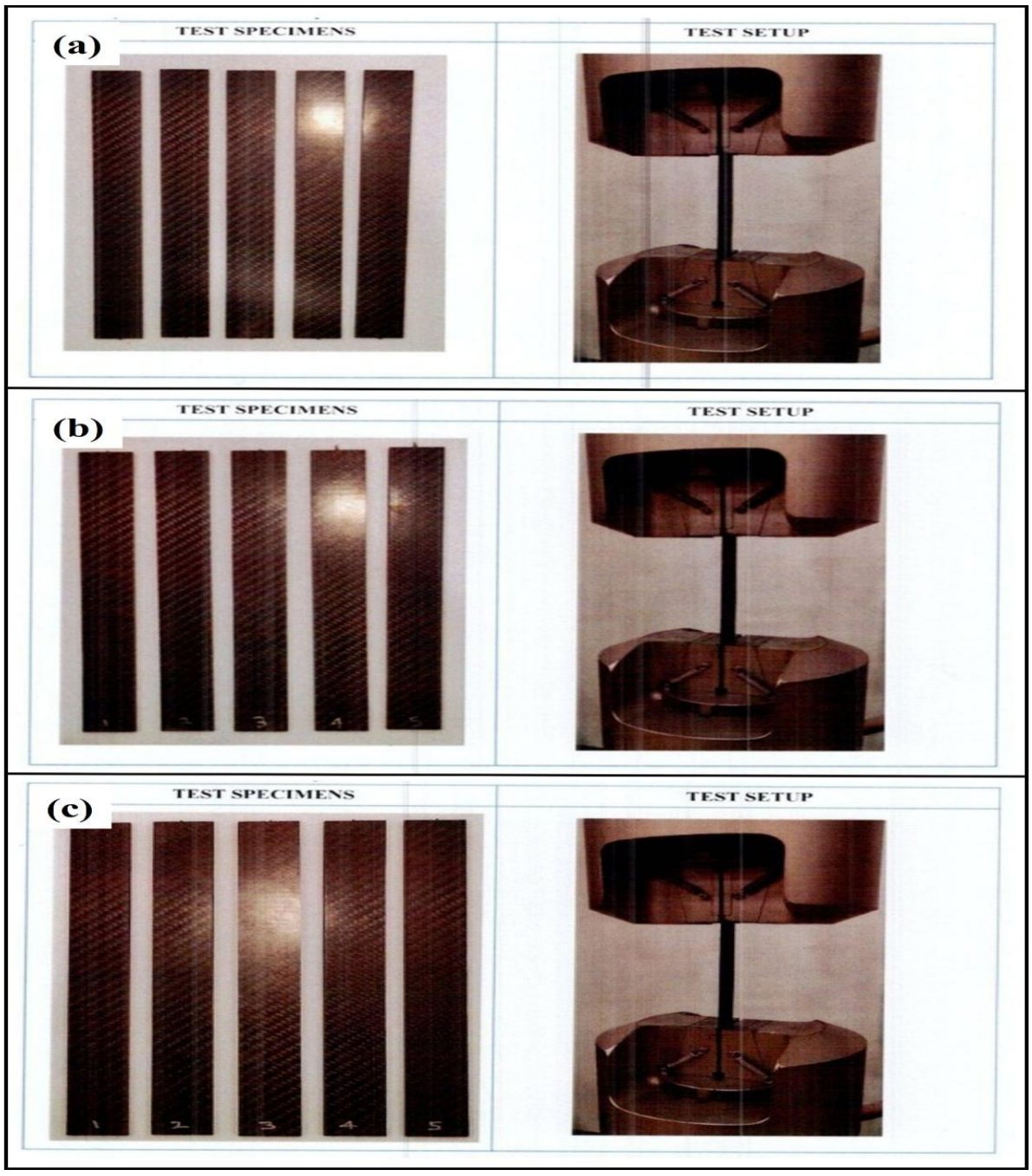



**Fig.2**. Tensile test configuration for CFRP specimens tested at (a) −10°C, (b) 40°C, and (c) 55°C in accordance with ASTM D3039-17.

Figure 3 illustrates the 3-point bending flexural test setup for CFRP according to ASTM D7264 at −10°C, 40°C, and 55°C. In Figure 3a, the beam is loaded after cold conditioning; brittle fracture is expected due to stiffened resin. Figure 3b represents the ambient test, where the specimen displays normal flexural behavior with expected deflection. In Figure 3c, the specimen

Corresponding author: Juneed Yawar, Juneedyawar@nitsri.ac.in

is tested at 55°C, where softened resin may increase ductility and energy absorption before failure. Each configuration shows correct span length and loading geometry, validating flexural test consistency across temperatures.

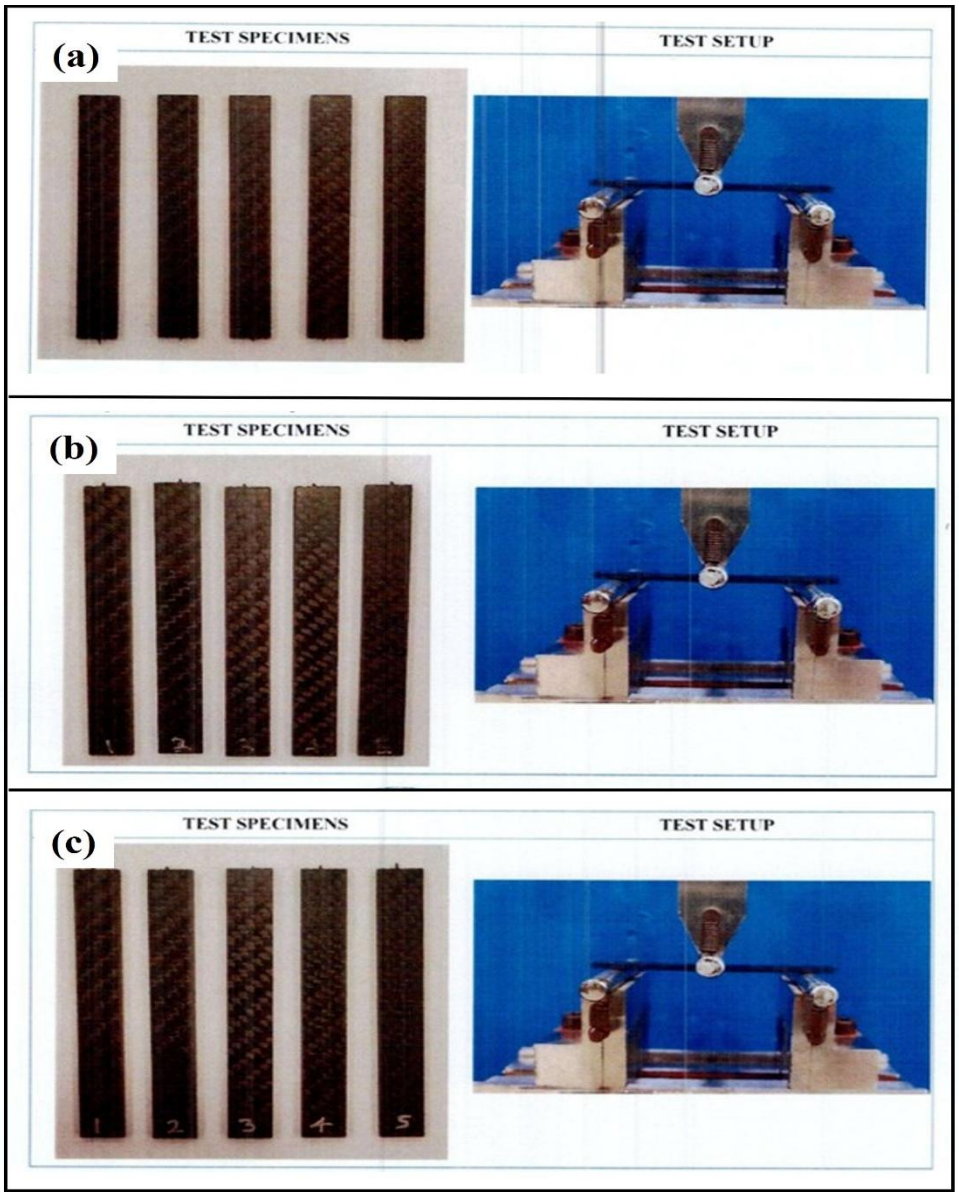



**Fig.3.** Flexural test setup for CFRP at (a) −10°C, (b) 40°C, and (c) 55°C following ASTM D7264 three-point bending procedure.

Figure 4 depicts the short-beam shear test arrangement for CFRP as per ASTM D2344. In Figure 4a, the specimen at −10°C undergoes loading that leads to rapid interlaminar fracture due to brittle resin. Figure 4b illustrates the standard ambient test at 40°C, showing a clean shear zone

Corresponding author: Juneed Yawar, Juneedyawar@nitsri.ac.in

influenced by balanced matrix and fiber properties. Figure 4c shows the 55°C test where matrix softening allows gradual shear damage, demonstrating how elevated temperature impacts interlayer bonding. Proper support placement and loading ensure valid measurement of shear strength across conditions.

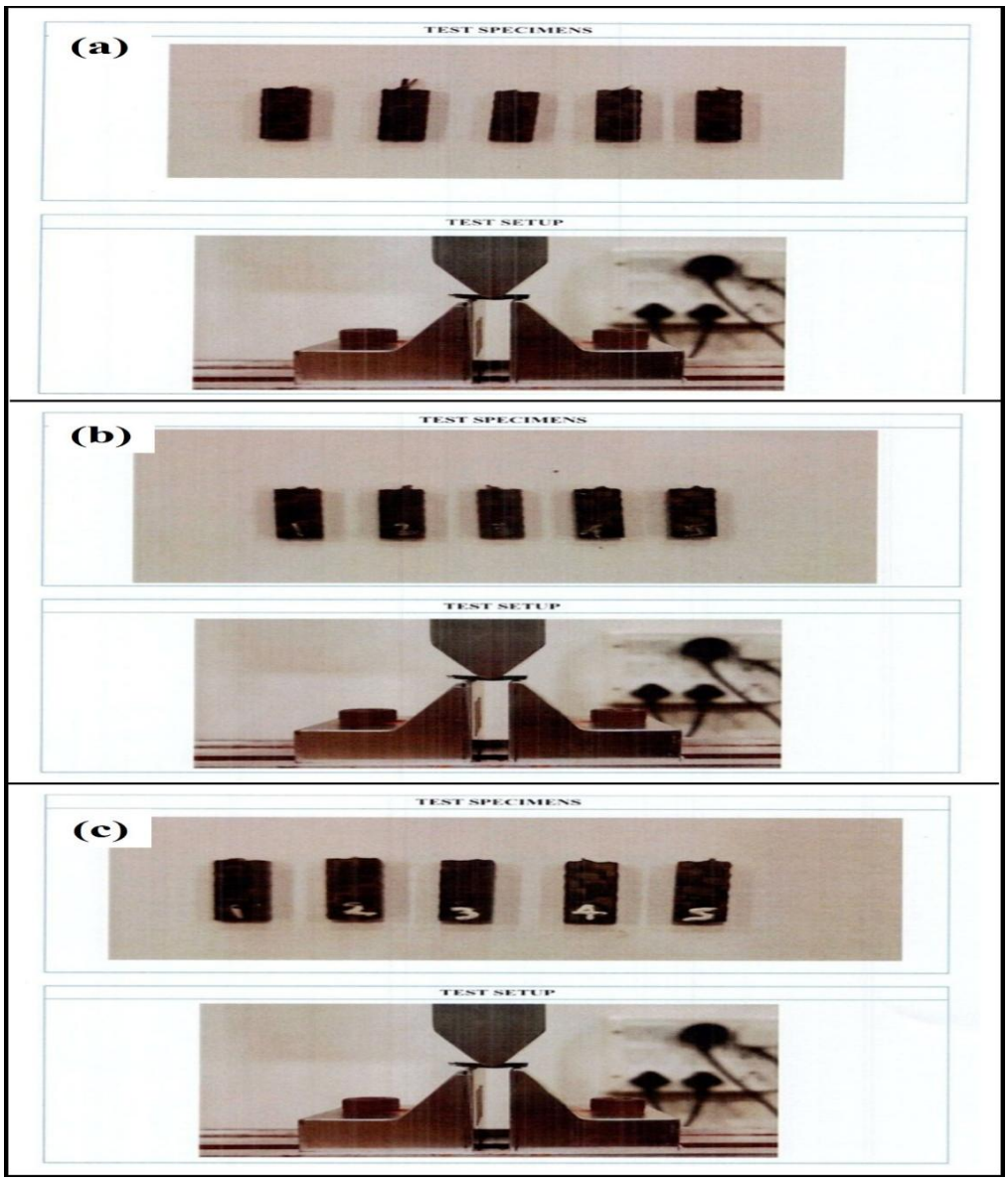



**Fig.4.** Short-beam shear test configuration for CFRP specimens at (a) −10°C, (b) 40°C, and (c) 55°C as per ASTM D2344.

Figure 5 shows the tensile test setup for PETG samples following ASTM D638-14 under −10°C, 40°C, and 55°C. In Figure 5a, the cold-conditioned PETG specimen is brittle and

Corresponding author: Juneed Yawar, Juneedyawar@nitsri.ac.in

vulnerable to sudden fracture. Figure 5b depicts testing at 40°C, where the polymer shows standard tensile behavior with moderate elongation. Figure 5c represents the test at 55°C, where PETG softens significantly and may exhibit necking or ductile failure. In all setups, proper clamping and alignment are maintained to isolate tensile behavior without introducing bending effects.

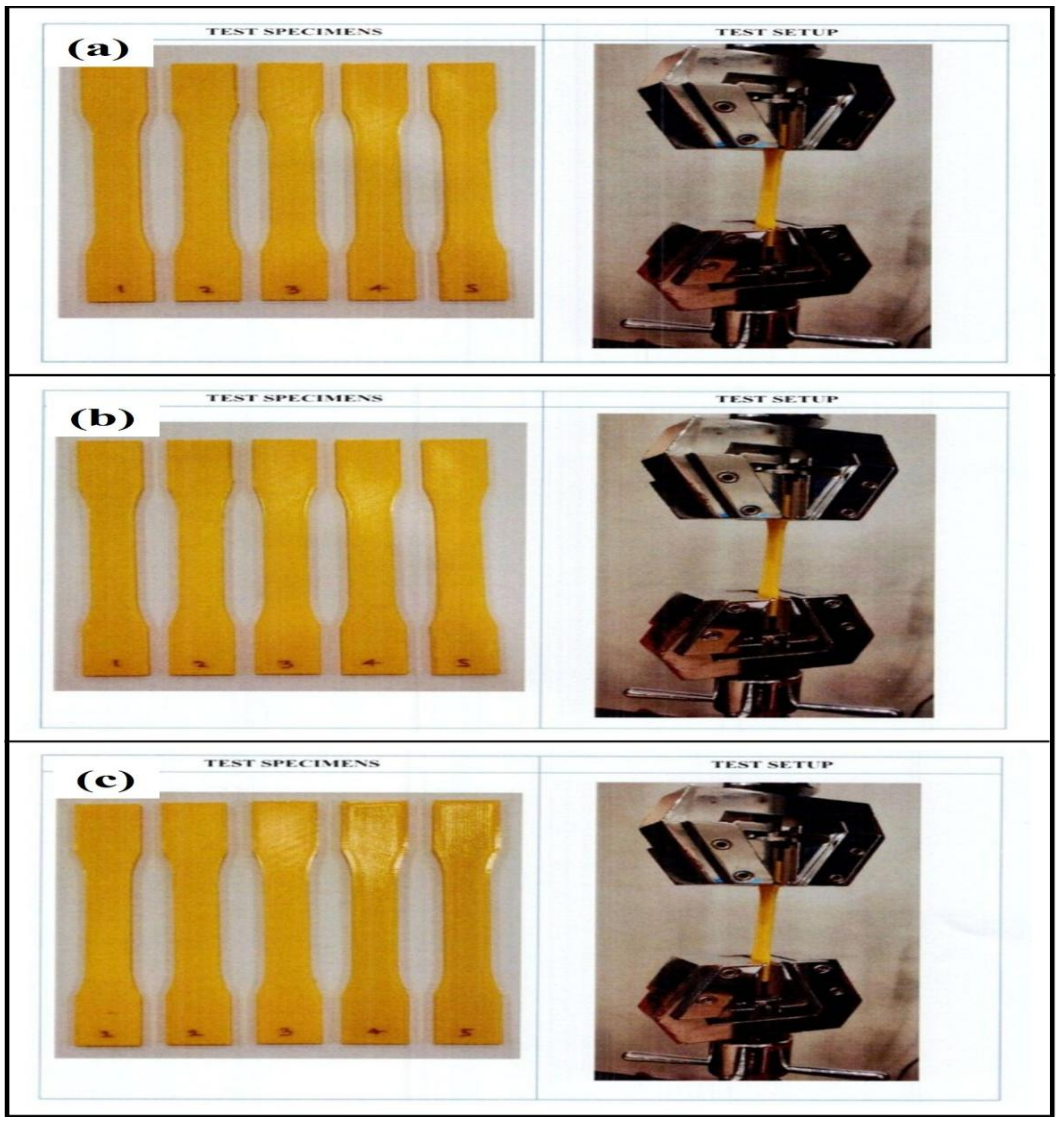



**Fig.5.** Tensile testing setup for PETG samples at (a) −10°C, (b) 40°C, and (c) 55°C conducted according to ASTM D638-14.

## 3. RESULTS AND DISCUSSION

### *3.1 Tensile Strength Analysis*

Corresponding author: Juneed Yawar, Juneedyawar@nitsri.ac.in

Tensile strength data for CFRP and PETG across the three thermal conditions (−10°C, 40°C, and 55°C) are presented in Tables 1 to 6 and Figures 6 to 11. These results allow a clear comparison of thermal sensitivity and mechanical stability between the two materials.

In Figure 6 and Table 1, CFRP at −10°C shows a steep linear stress–strain curve with a sharp drop after the peak, indicating brittle fracture behavior. The tensile strength ranges from 608.33 MPa to 647.29 MPa, averaging 633.39 MPa. This consistency confirms high stiffness and minimal variation between specimens. At subzero temperatures, the matrix becomes rigid, enhancing fiber-dominated load transfer. Compared to its tensile performance at 55°C (580.84 MPa), CFRP experiences a strength drop of 8.3%, indicating strong thermal stability and minimal matrix degradation over the tested temperature range. This characteristic is crucial for UAV frames operating at high altitudes, where mechanical reliability under low thermal conductivity is essential.

**Table 1.** CFRP tensile strength values at −10°C (ASTM D3039-17, 2 mm/min).

| Specimen | Width (mm) | Thickness (mm) | Tensile Strength (MPa) |
|---|---|---|---|
| 1 | 24.97 | 2.469 | 647.29 |
| 2 | 24.96 | 2.491 | 641.14 |
| 3 | 24.97 | 2.479 | 608.33 |
| 4 | 24.98 | 2.507 | 629.27 |
| 5 | 24.99 | 2.459 | 640.94 |

Corresponding author: Juneed Yawar, Juneedyawar@nitsri.ac.in

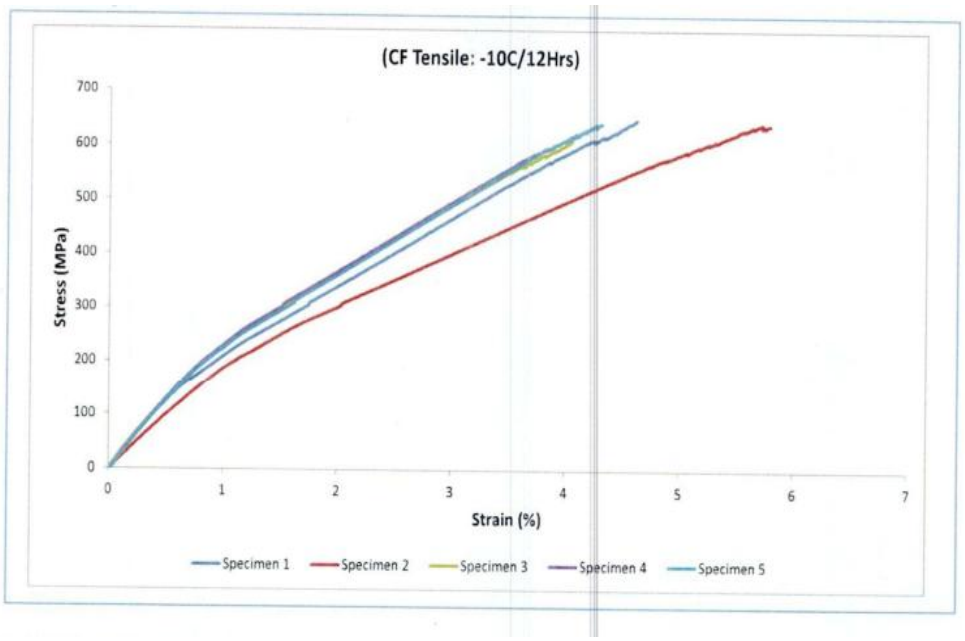



**Fig.6.** Tensile strength graph of CFRP at −10°C using ASTM D3039-17.

In contrast, Figure 7 and Table 2 show that PETG at −10°C behaves in a brittle manner. The curves are short and steep, with early failure and negligible elongation. Strength values fall between 32.63 MPa and 34.22 MPa. The fracture is abrupt, with no yielding, indicating that PETG vitrifies at low temperatures. This behavior could lead to catastrophic failure in UAV applications under cold-weather deployment.

**Table 2.** PETG tensile strength values at −10°C (ASTM D638-14, 50 mm/min).

| Specimen | Width (mm) | Thickness (mm) | Tensile Strength (MPa) |
|---|---|---|---|
| 1 | 12.849 | 3.146 | 32.63 |
| 2 | 12.838 | 3.158 | 33.54 |
| 3 | 12.844 | 3.148 | 34.22 |
| 4 | 12.887 | 3.131 | 32.74 |
| 5 | 12.873 | 3.094 | 34.03 |

Corresponding author: Juneed Yawar, Juneedyawar@nitsri.ac.in

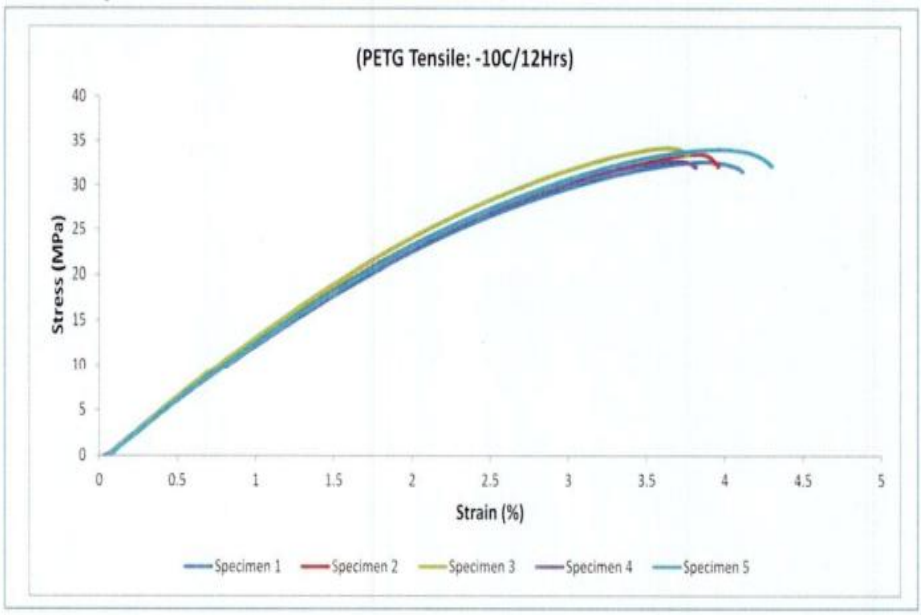



**Fig.7.** Tensile strength graph of PETG at −10°C using ASTM D638-14.

At 40°C, CFRP's tensile performance remains strong. Figure 8 and Table 3 show a tensile strength range of 610.32 MPa to 673.99 MPa, with an average of 648.21 MPa. The curves remain sharply linear but with slightly softer failure slopes, suggesting matrix plasticity onset. This moderate change reflects excellent thermal resilience, with less than 3% strength fluctuation. For UAVs operating in ambient conditions, this demonstrates CFRP's reliability in maintaining structural stiffness and resisting deformation.

**Table 3.** CFRP tensile strength values at 40°C (ASTM D3039-17, 2 mm/min).

| Specimen | Width (mm) | Thickness (mm) | Tensile Strength (MPa) |
|---|---|---|---|
| 1 | 25.02 | 2.495 | 639.62 |
| 2 | 24.97 | 2.554 | 673.99 |
| 3 | 25.03 | 2.471 | 656.51 |
| 4 | 25.05 | 2.508 | 610.32 |
| 5 | 25.06 | 2.503 | 642.05 |

Corresponding author: Juneed Yawar, Juneedyawar@nitsri.ac.in

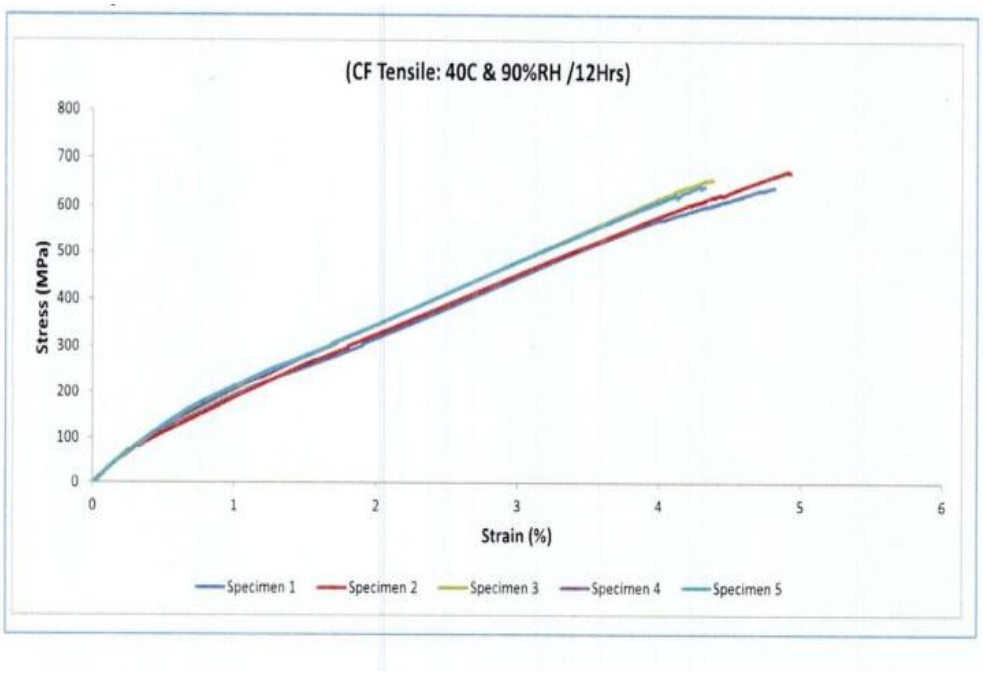



**Fig.8.** Tensile strength graph of CFRP at 40°C using ASTM D3039-17.

Figure 9 and Table 4 show that PETG at 40°C undergoes a transition from brittle to semi-ductile behavior. Specimen strength drops to between 26.06 MPa and 26.98 MPa — an approximate 20% reduction from its −10°C condition. Specifically, PETG's tensile strength dropped from 33.23 MPa at −10°C to 26.52 MPa at 40°C, a 20.2% reduction, highlighting its vulnerability to thermal softening. The curves elongate slightly, indicating improved strain-to-failure. This behavior may help absorb some mechanical energy during impact but also marks the beginning of significant softening, which raises concerns for structural UAV use.

**Table 4.** PETG tensile strength values at 40°C (ASTM D638-14, 50 mm/min).

| Specimen | Width (mm) | Thickness (mm) | Tensile Strength (MPa) |
|---|---|---|---|
| 1 | 12.872 | 3.130 | 26.60 |
| 2 | 12.948 | 3.156 | 26.21 |
| 3 | 12.867 | 3.158 | 26.06 |
| 4 | 12.876 | 3.159 | 26.21 |
| 5 | 12.882 | 3.071 | 26.98 |

Corresponding author: Juneed Yawar, Juneedyawar@nitsri.ac.in

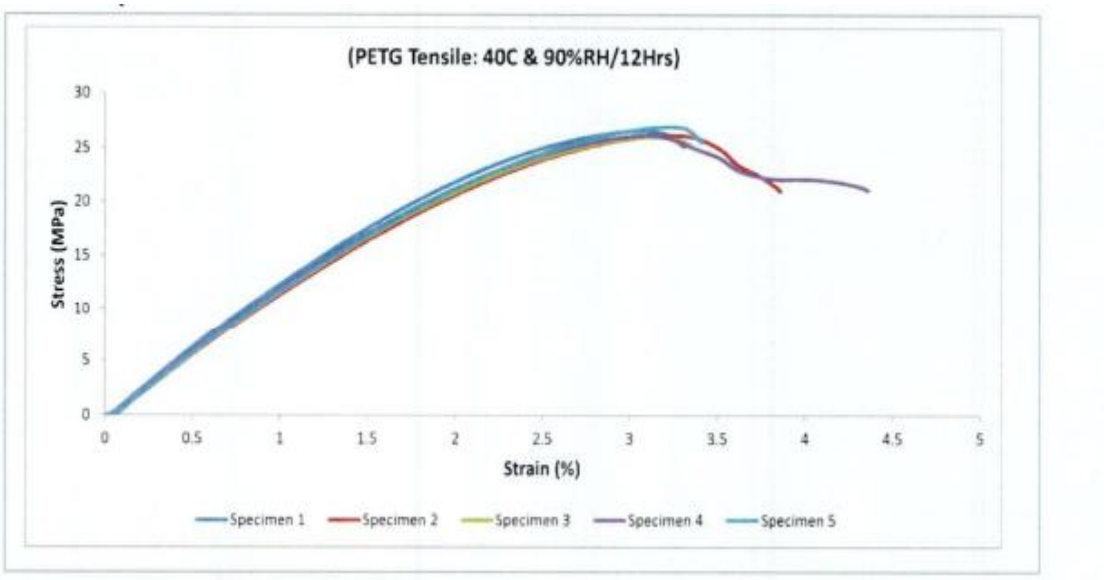



**Fig.9.** Tensile strength graph of PETG at 40°C using ASTM D638-14.

At 55°C, Figure 10 and Table 5 show that CFRP maintains tensile strength between 548.69 MPa and 613.88 MPa, averaging 580.84 MPa. The slope of the curve remains steep, though the fracture becomes less abrupt. The matrix clearly softens, but the fiber reinforcement compensates effectively. The total drop from −10°C to 55°C remains within 8.3%, indicating excellent load-carrying capacity even in thermally challenging UAV environments like desert operations or hot-ground exposure.

**Table 5.** CFRP tensile strength values at 55°C (ASTM D3039-17, 2 mm/min).

| Specimen | Width (mm) | Thickness (mm) | Tensile Strength (MPa) |
|---|---|---|---|
| 1 | 25.09 | 2.514 | 590.16 |
| 2 | 25.10 | 2.521 | 613.88 |
| 3 | 25.06 | 2.551 | 610.73 |
| 4 | 25.07 | 2.546 | 548.69 |
| 5 | 25.11 | 2.534 | 567.53 |

Corresponding author: Juneed Yawar, Juneedyawar@nitsri.ac.in

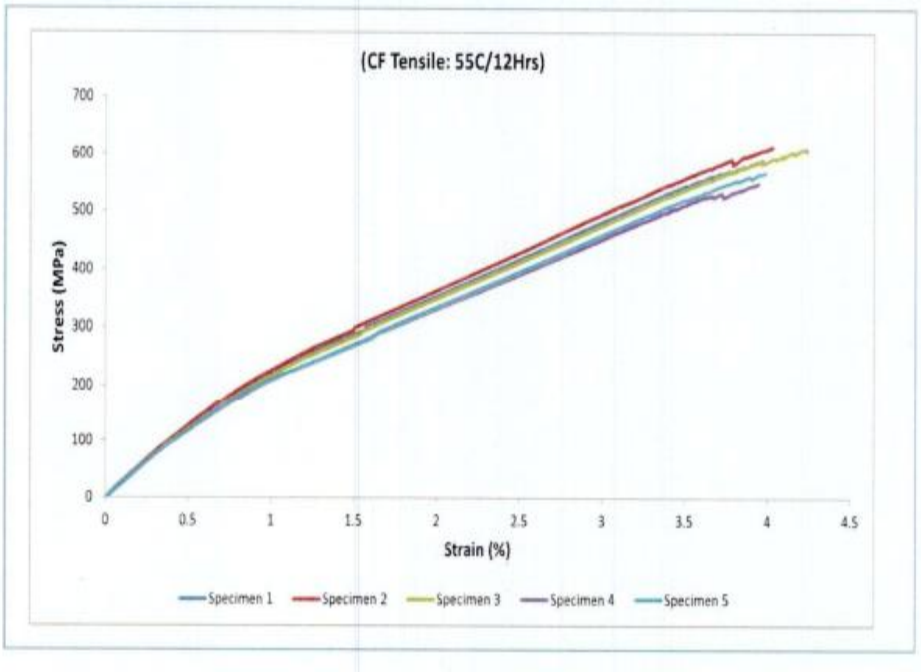



**Fig.10.** Tensile strength graph of CFRP at 55°C using ASTM D3039-17.

Finally, Figure 11 and Table 6 show PETG's lowest performance at 55°C. Strength values range from 26.37 MPa to 32.74 MPa. The stress–strain curves show long extensions before failure, highlighting significant ductile deformation, necking, and plastic flow. Although this suggests some impact tolerance, it also indicates structural instability. The loss of stiffness and yield strength makes PETG unsuitable for UAV primary structures, especially where high load-to-weight efficiency is critical. Although the average strength at 55°C (29.56 MPa) slightly exceeds the 40°C condition, the net reduction from −10°C still accounts for a 11.1% loss, reinforcing the material's limited high-temperature capability.

In summary, CFRP demonstrates superior tensile performance across all temperatures with a total drop of only ~8.3% from −10°C to 55°C, maintaining structural integrity and stiffness. PETG, in contrast, shows a significant 20–25% reduction in strength and a clear shift from brittle to ductile fracture, making it more applicable to non-critical, low-stress UAV components or disposable structural elements.

**Table 6.** PETG tensile strength values at 55°C (ASTM D638-14, 50 mm/min).

Corresponding author: Juneed Yawar, Juneedyawar@nitsri.ac.in

| Specimen | Width (mm) | Thickness (mm) | Tensile Strength (MPa) |
|---|---|---|---|
| 1 | 12.861 | 3.071 | 32.74 |
| 2 | 12.870 | 3.110 | 28.26 |
| 3 | 12.808 | 3.169 | 29.81 |
| 4 | 12.929 | 3.289 | 26.37 |
| 5 | 12.985 | 3.317 | 28.59 |

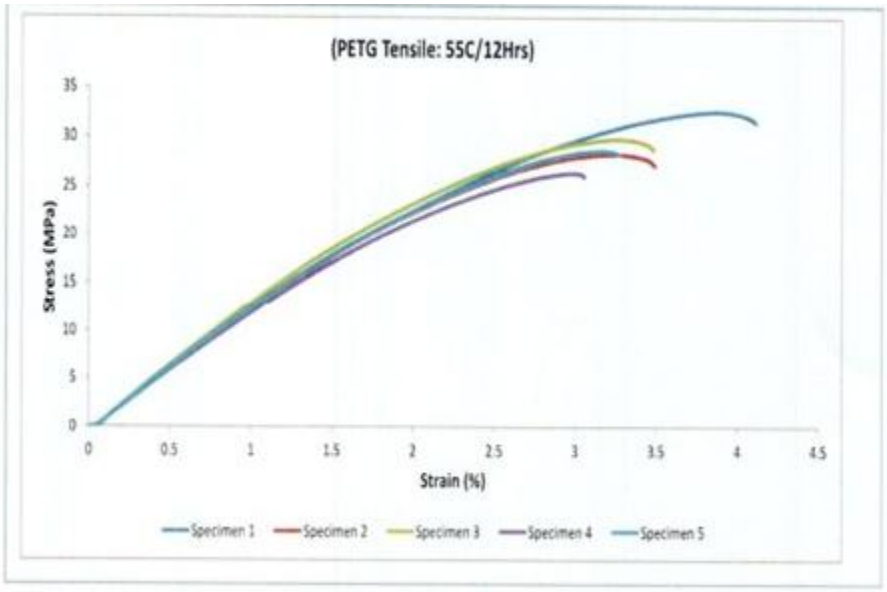



**Fig.11.** Tensile strength graph of PETG at 55°C using ASTM D638-14.

*3.2 Flexural and Shear Performance of CFRP*

Flexural and short-beam shear test results for CFRP under varying thermal conditions are shown in Figures 12 to 17 and Tables 7 to 12. These results evaluate the bending and interlaminar stability of the material, both essential for UAV frame applications [55].

At −10°C, CFRP displays high flexural strength, as shown in Figure 12 and Table 7. Specimen values range from 232.06 MPa to 259.69 MPa, averaging 245.36 MPa. The stress–strain curve rises steeply and fractures abruptly, typical of brittle matrix failure at low temperature. This suggests limited energy absorption but high rigidity, suitable for load-bearing UAV structures.

**Table 7.** CFRP flexural strength values at −10°C (ASTM D7264, 1 mm/min).

Corresponding author: Juneed Yawar, Juneedyawar@nitsri.ac.in

| Specimen | Width (mm) | Thickness (mm) | Flexural Strength (MPa) |
|---|---|---|---|
| 1 | 13.028 | 2.452 | 397.72 |
| 2 | 13.007 | 2.424 | 438.73 |
| 3 | 13.015 | 2.548 | 492.05 |
| 4 | 13.021 | 2.537 | 347.13 |
| 5 | 13.017 | 2.459 | 447.82 |

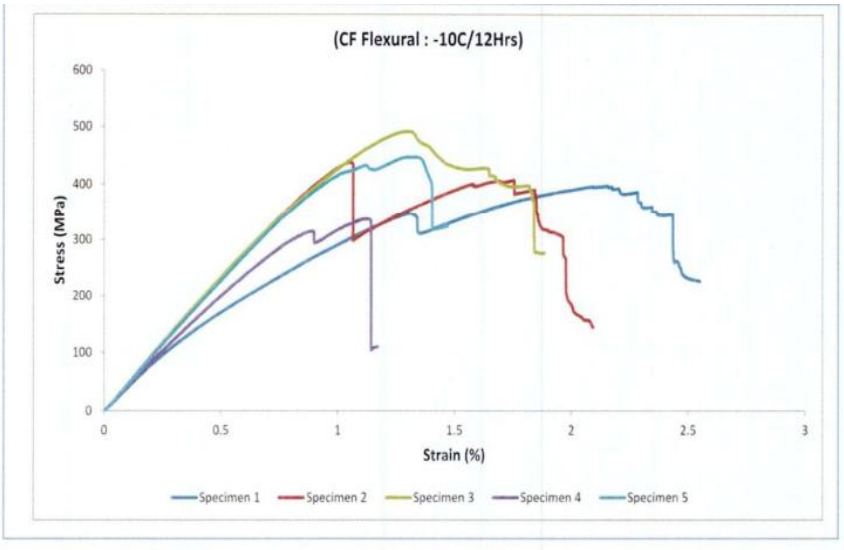



**Fig.12.** Flexural strength graph of CFRP at −10°C using ASTM D7264.

As the temperature increases to 40°C, Figure 13 and Table 8 show a slight decrease in flexural strength, with an average of 235.67 MPa. The curve flattens slightly post-peak, suggesting minor matrix softening. Specimens fail more gradually, indicating better energy dissipation, yet the stiffness remains predominantly fiber-controlled.

**Table 8.** CFRP flexural strength values at 40°C (ASTM D7264, 1 mm/min).

| Specimen | Width (mm) | Thickness (mm) | Flexural Strength (MPa) |
|---|---|---|---|
| 1 | 13.021 | 2.488 | 330.13 |
| 2 | 13.031 | 2.426 | 350.02 |

Corresponding author: Juneed Yawar, Juneedyawar@nitsri.ac.in

| | | | |
|---|---|---|---|
| 3 | 13.040 | 2.538 | 439.26 |
| 4 | 13.018 | 2.438 | 341.39 |
| 5 | 13.015 | 2.460 | 395.39 |

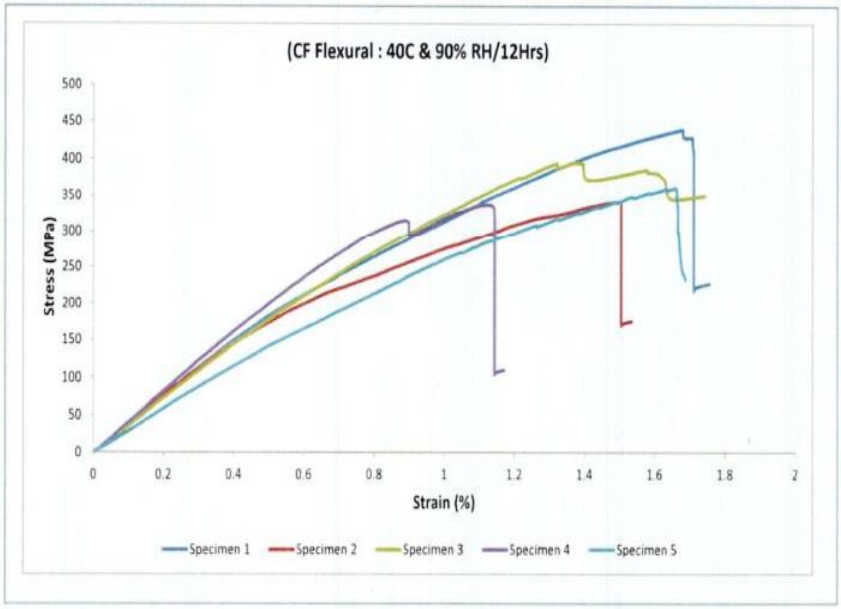



**Fig.13.** Flexural strength graph of CFRP at 40°C using ASTM D7264.

At 55°C, the flexural strength drops further to an average of 221.58 MPa (Figure 14, Table 9). This reduction from 245.36 MPa at −10°C to 221.58 MPa at 55°C reflects a 9.7% decrease in flexural strength, attributed primarily to matrix softening. While this reflects a modest decrease, the structural integrity of the CFRP remains intact. The curve broadens slightly, failure becomes less abrupt, but no fiber delamination or catastrophic breakage is observed.

**Table 9.** CFRP flexural strength values at 55°C (ASTM D7264, 1 mm/min).

| **Specimen** | **Width (mm)** | **Thickness (mm)** | **Flexural Strength (MPa)** |
|---|---|---|---|
| 1 | 12.948 | 2.530 | 246.97 |
| 2 | 12.971 | 2.557 | 362.59 |
| 3 | 12.944 | 2.576 | 337.13 |
| 4 | 13.062 | 2.539 | 276.17 |

Corresponding author: Juneed Yawar, Juneedyawar@nitsri.ac.in

| | | | |
|---|---|---|---|
| 5 | 12.972 | 2.559 | 361.02 |

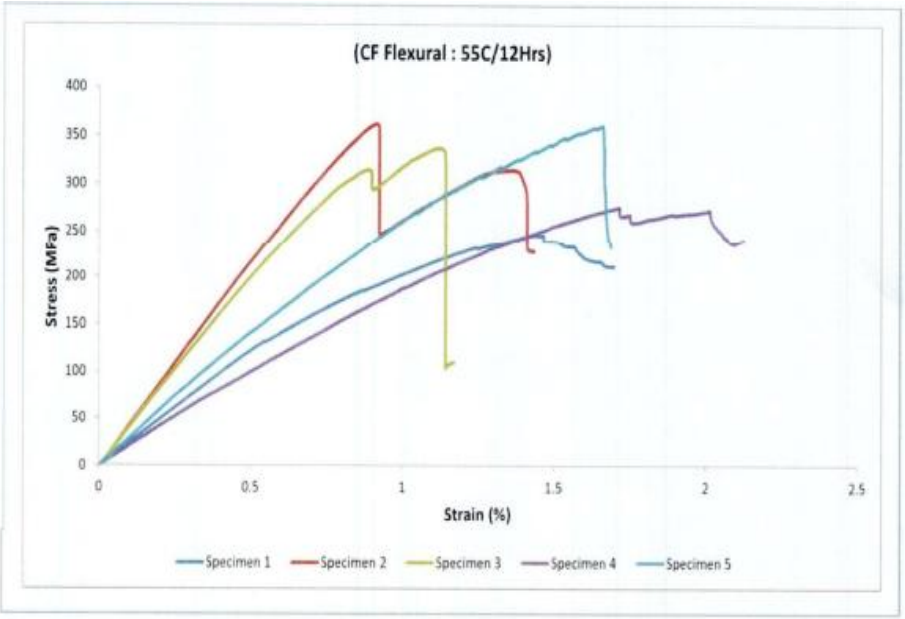



**Fig.14.** Flexural strength graph of CFRP at 55°C using ASTM D7264.

Interlaminar shear behavior follows a similar pattern. At −10°C, Figure 15 and Table 10 show average shear strength of 84.53 MPa, with abrupt load drops typical of brittle matrix behavior. As temperature increases to 40°C (Figure 16, Table 11), shear strength slightly reduces to 79.12 MPa. The failure curves round out, reflecting a transition to more ductile matrix behavior. At 55°C, Figure 17 and Table 12 show the lowest shear performance, averaging 72.45 MPa. The interlaminar shear strength drops from 84.53 MPa at −10°C to 72.45 MPa at 55°C, showing a 14.3% decrease, which represents the largest degradation among the three test types for CFRP. Though matrix softening is evident, cohesive failure modes persist, and no fiber detachment occurs.

Overall, CFRP's flexural and interlaminar strength decline moderately with temperature ~9.7% and ~14.3% respectively — but the material maintains strong load-bearing and bonding characteristics. These results confirm CFRP's viability for UAV components exposed to out-of-plane bending, aerodynamic stress, and structural vibrations across a range of operating environments.

Corresponding author: Juneed Yawar, Juneedyawar@nitsri.ac.in

**Table 10.** CFRP shear strength values at −10°C (ASTM D2344, 1 mm/min).

| Specimen | Width (mm) | Thickness (mm) | Short Beam Strength (MPa) |
|---|---|---|---|
| 1 | 4.975 | 2.564 | 268.83 |
| 2 | 5.087 | 2.541 | 254.17 |
| 3 | 5.116 | 2.542 | 269.56 |
| 4 | 5.013 | 2.530 | 293.02 |
| 5 | 5.066 | 2.611 | 281.79 |

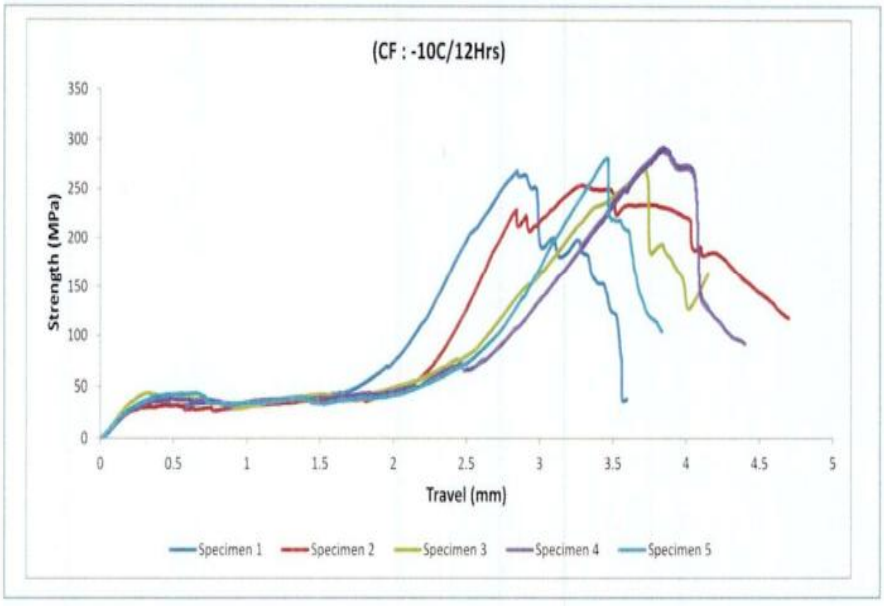



**Fig.15.** Interlaminar shear strength graph of CFRP at −10°C using ASTM D2344.

**Table 11.** CFRP shear strength values at 40°C (ASTM D2344, 1 mm/min).

| Specimen | Width (mm) | Thickness (mm) | Short Beam Strength (MPa) |
|---|---|---|---|
| 1 | 5.092 | 2.482 | 233.62 |
| 2 | 5.060 | 2.607 | 235.25 |
| 3 | 5.018 | 2.574 | 259.02 |
| 4 | 5.126 | 2.547 | 252.60 |

Corresponding author: Juneed Yawar, Juneedyawar@nitsri.ac.in

| | | | |
|---|---|---|---|
| 5 | 4.972 | 2.581 | 247.73 |

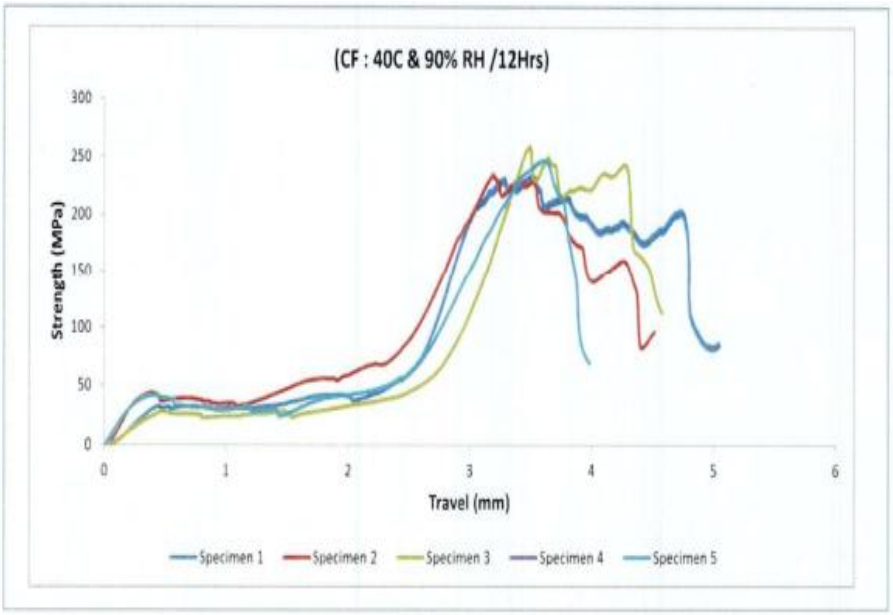



**Fig.16.** Interlaminar shear strength graph of CFRP at 40°C using ASTM D2344.

**Table 12.** CFRP shear strength values at 55°C (ASTM D2344, 1 mm/min).

| **Specimen** | **Width (mm)** | **Thickness (mm)** | **Short Beam Strength (MPa)** |
|---|---|---|---|
| 1 | 4.980 | 2.602 | 188.25 |
| 2 | 5.001 | 2.523 | 212.28 |
| 3 | 5.010 | 2.584 | 246.73 |
| 4 | 5.051 | 2.588 | 229.07 |
| 5 | 5.010 | 2.584 | 218.81 |

Corresponding author: Juneed Yawar, Juneedyawar@nitsri.ac.in

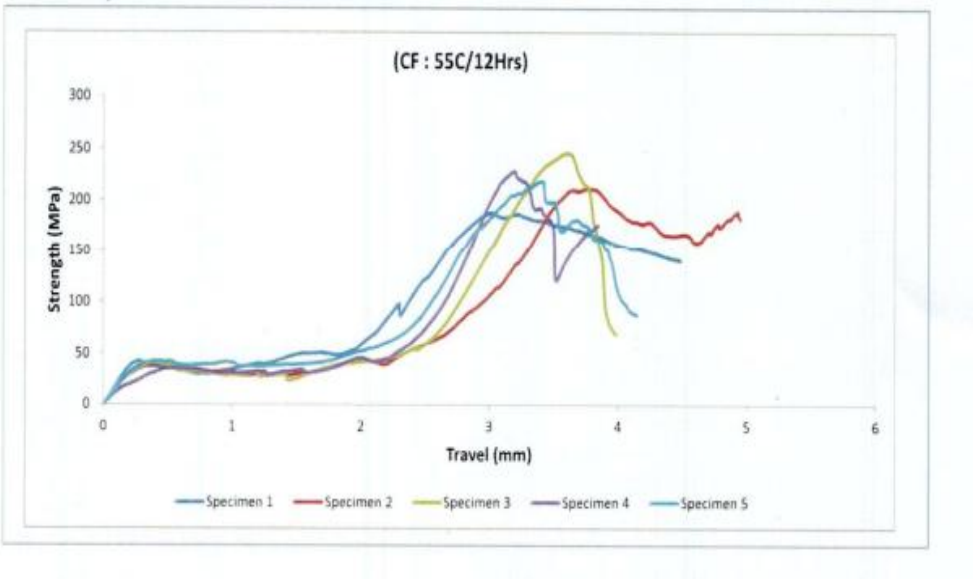



**Fig.17.** Interlaminar shear strength graph of CFRP at 55°C using ASTM D2344.

*3.3 Fracture Behavior of PETG*

PETG samples demonstrated a clear transition in fracture behavior across the thermal range, supported by tensile results in Figures 7, 9, and 11 and raw strength data in Tables 2, 4, and 6.

At −10°C, PETG exhibited brittle fracture. Figure 7 and Table 2 show short, steep stress–strain curves with early failure. Strength values range between 32.63 MPa and 34.22 MPa, with an average of 33.23 MPa. The fracture surfaces are smooth and clean, characteristic of crack propagation without significant plastic flow. The material enters a glassy state at this temperature, restricting molecular mobility and increasing failure risk under sudden loading — a disadvantage for UAVs exposed to cold airspace.

At 40°C, a significant transition is observed. Figure 9 and Table 4 show that PETG's tensile strength drops to an average of 26.52 MPa. This drop from 33.23 MPa at −10°C corresponds to a 20.2% reduction in strength. The stress–strain curve lengthens, and necking becomes visible.

Fracture surfaces begin to show whitening and roughness, indicating increased energy absorption prior to failure. While ductility improves, strength diminishes — a trade-off that complicates PETG’s role in UAV frame elements.

Corresponding author: Juneed Yawar, Juneedyawar@nitsri.ac.in

At 55°C, Figure 11 and Table 6 reveal PETG's most ductile behavior. Curves are long and flattened, fracture points are delayed, and the material undergoes substantial elongation before failure. Strength values range from 26.37 MPa to 32.74 MPa, averaging 29.56 MPa. The stress–strain response at this temperature reflects necking, whitening, and surface crazing prior to rupture. Although the average strength at 55°C (29.56 MPa) is slightly higher than at 40°C, the net reduction from −10°C still amounts to a 11.1% drop, confirming a consistent loss of load-bearing capacity due to thermal softening.

In conclusion, PETG transitions from brittle to fully ductile behavior as temperature increases, but this shift comes at the cost of measurable strength reduction. The dual effect of decreasing tensile strength and increasing ductility makes PETG a poor choice for UAV structural frames, particularly those exposed to cyclic or high-temperature conditions. It may remain suitable for enclosures or low-stress non-structural components, but its thermal instability limits its reliability for primary UAV load-bearing applications.

## 4. CONCLUSION

This study presents a comprehensive thermomechanical assessment of Carbon Fiber Reinforced Polymer and Polyethylene Terephthalate Glycol for UAV frame applications across varying thermal environments. Standardized ASTM protocols were used to evaluate tensile, flexural, and shear properties at −10°C, 40°C, and 55°C, simulating real UAV operational extremes.

CFRP demonstrated excellent structural reliability, retaining 91.7% of its tensile strength across the temperature range. Flexural and shear strengths declined by 9.7% and 14.3%, respectively. Fracture surfaces indicated brittle failure at low temperatures and controlled matrix softening at elevated conditions, without fiber delamination. These results validate CFRP's superior thermal resilience and make it well-suited for UAV primary structures that require consistent mechanical performance under thermal cycling.

In contrast, PETG exhibited higher thermal sensitivity, with tensile strength dropping by 20.2% at 40°C and 11.1% at 55°C. It also showed a distinct transition from brittle to ductile behavior, accompanied by reduced stiffness and increased plastic deformation. While cost-

Corresponding author: Juneed Yawar, Juneedyawar@nitsri.ac.in

effective and suitable for additive manufacturing, PETG's thermal instability limits its use to secondary, non-load-bearing UAV components.

The findings correlate strength degradation with temperature-induced matrix behavior and are supported by detailed graphical trends in Figures 6–17 and the comparative summary in Figure 18. This work not only delivers high-fidelity material data but also offers a reproducible framework for evaluating UAV structural materials under real service conditions.

Future studies may explore fatigue behavior, hybrid reinforcement strategies, and thermal-aging simulations to extend these results to long-term UAV performance scenarios.

ACKNOWLEDGEMENTS

The authors gratefully acknowledge the Department of Mechanical Engineering, National Institute of Technology Srinagar, for providing research infrastructure and guidance throughout this work. The authors also extend their sincere thanks to Eagle Eye Drones, Mysore–Bangalore, for granting access to laboratory facilities and supporting drone-related experimental work. The technical and experimental assistance provided by both institutions was instrumental in the successful completion of this study.

DECLARATION OF CONFLICTING INTERESTS

The author(s) declare that they have no known competing financial interests or personal relationships that could have appeared to influence the work reported in this paper.

FUNDING

The author(s) received no financial support for the research, authorship, and/or publication of this article.

**REFERENCE**

[1] H. Guo, M. Li, P. Sun, C. Zhao, W. Zuo, and X. Li, "Lightweight and maintainable rotary-wing UAV frame from configurable design to detailed design," *Advances in Mechanical Engineering,* vol. 13, no. 7, p. 16878140211034999, 2021.

[2] H. X. Zhou and B. Liu, "Characteristics analysis and optimization of flying-wing vehicle structure," *Advanced Materials Research,* vol. 1077, pp. 177-184, 2015.

Corresponding author: Juneed Yawar, Juneedyawar@nitsri.ac.in

[3] S. Xu, Y. Liu, J. Zhang, and Y. Zheng, "Preliminary Design and Optimization of Primary Structures for a Tilt-Duct UAV," *Aerospace,* vol. 11, no. 4, p. 286, 2024.

[4] A. M. Rayed, B. Esakki, A. Ponnambalam, S. C. Banik, and K. Aly, "Optimization of UAV structure and evaluation of vibrational and fatigue characteristics through simulation studies," *International Journal for Simulation and Multidisciplinary Design Optimization,* vol. 12, p. 17, 2021.

[5] V. A. Kumar, M. Sivaguru, B. R. Janaki, K. S. Eswar, P. Kiran, and R. Vijayanandh, "Structural optimization of frame of the multi-rotor unmanned aerial vehicle through computational structural analysis," in *Journal of Physics: Conference Series*, 2021, vol. 1849, no. 1: IOP Publishing, p. 012004.

[6] S. K. Moon, Y. E. Tan, J. Hwang, and Y.-J. Yoon, "Application of 3D printing technology for designing light-weight unmanned aerial vehicle wing structures," *International journal of precision engineering and manufacturing-green technology,* vol. 1, pp. 223-228, 2014.

[7] L. Song *et al.*, "An all-movable rudder designed by thermo-elastic topology optimization and manufactured by additive manufacturing," *Computers & Structures,* vol. 243, p. 106405, 2021.

[8] S. A. H. Mohsan, M. A. Khan, F. Noor, I. Ullah, and M. H. Alsharif, "Towards the unmanned aerial vehicles (UAVs): A comprehensive review," *Drones,* vol. 6, no. 6, p. 147, 2022.

[9] M. T. Yavuz and I. Ozkol, "Thermal Structural Design Aspects of Military Aircraft," *Journal of Aeronautics and Space Technologies,* vol. 17, no. 1, pp. 124-158, 2024.

[10] S. A. H. Mohsan, N. Q. H. Othman, Y. Li, M. H. Alsharif, and M. A. Khan, "Unmanned aerial vehicles (UAVs): Practical aspects, applications, open challenges, security issues, and future trends," *Intelligent service robotics,* vol. 16, no. 1, pp. 109-137, 2023.

[11] G. D. Goh, S. Agarwala, G. L. Goh, V. Dikshit, S. L. Sing, and W. Y. Yeong, "Additive manufacturing in unmanned aerial vehicles (UAVs): Challenges and potential," *Aerospace Science and Technology,* vol. 63, pp. 140-151, 2017.

[12] N. Elmeseiry, N. Alshaer, and T. Ismail, "A detailed survey and future directions of unmanned aerial vehicles (uavs) with potential applications," *Aerospace,* vol. 8, no. 12, p. 363, 2021.

Corresponding author: Juneed Yawar, Juneedyawar@nitsri.ac.in

[13] H. A. Hashim, "Advances in UAV avionics systems architecture, classification and integration: A comprehensive review and future perspectives," *Results in Engineering,* p. 103786, 2024.

[14] G. Rathinakumar and E. L. Ntantis, "Designing a Quadcopter for Fire and Temperature Detection with an Infrared Camera and PIR Sensor," *Drones and Autonomous Vehicles,* vol. 1, no. 2, p. 10003, 2024.

[15] T. Omar and M. L. Nehdi, "Remote sensing of concrete bridge decks using unmanned aerial vehicle infrared thermography," *Automation in Construction,* vol. 83, pp. 360-371, 2017.

[16] A. Michail *et al.*, "A comprehensive review of unmanned aerial vehicle-based approaches to support photovoltaic plant diagnosis," *Heliyon,* vol. 10, no. 1, 2024.

[17] Y. Alghamdi, A. Munir, and H. M. La, "Architecture, classification, and applications of contemporary unmanned aerial vehicles," *IEEE Consumer Electronics Magazine,* vol. 10, no. 6, pp. 9-20, 2021.

[18] T. Omar and M. L. Nehdi, "Thermal detection of subsurface delaminations in reinforced concrete bridge decks using unmanned aerial vehicle," *Spec. Publ,* vol. 331, pp. 1-14, 2019.

[19] P. Singh, M. A. Ansari, and A. Bisoi, "An analytical analysis of vibrational energy harvesting using piezoelectric energy harvester in a fixed wing unmanned aerial vehicle," *Proceedings of the Institution of Mechanical Engineers, Part L: Journal of Materials: Design and Applications,* vol. 238, no. 8, pp. 1514-1525, 2024.

[20] N. Van de Werken, H. Tekinalp, P. Khanbolouki, S. Ozcan, A. Williams, and M. Tehrani, "Additively manufactured carbon fiber-reinforced composites: State of the art and perspective," *Additive Manufacturing,* vol. 31, p. 100962, 2020.

[21] B. A. Alshammari *et al.*, "Comprehensive review of the properties and modifications of carbon fiber-reinforced thermoplastic composites," *Polymers,* vol. 13, no. 15, p. 2474, 2021.

[22] G. Barra, L. Guadagno, M. Raimondo, M. G. Santonicola, E. Toto, and S. Vecchio Ciprioti, "A comprehensive review on the thermal stability assessment of polymers and composites for aeronautics and space applications," *Polymers,* vol. 15, no. 18, p. 3786, 2023.

[23] S. Kesarwani, "Polymer composites in aviation sector," *Int. J. Eng. Res,* vol. 6, no. 10, 2017.

Corresponding author: Juneed Yawar, Juneedyawar@nitsri.ac.in

[24] G. D. Goh, W. Toh, Y. Yap, T. Ng, and W. Yeong, "Additively manufactured continuous carbon fiber-reinforced thermoplastic for topology optimized unmanned aerial vehicle structures," *Composites Part B: Engineering,* vol. 216, p. 108840, 2021.

[25] S. M. F. B. S. Hairi, S. J. M. B. M. Saleh, A. H. Ariffin, and Z. B. Omar, "A Review on Composite Aerostructure Development for UAV Application," *Green Hybrid Composite in Engineering and Non-Engineering Applications,* pp. 137-157, 2023.

[26] D. Ozkan, M. S. Gok, and A. C. Karaoglanli, "Carbon fiber reinforced polymer (CFRP) composite materials, their characteristic properties, industrial application areas and their machinability," *Engineering Design Applications III: Structures, Materials and Processes,* pp. 235-253, 2020.

[27] S. Hegde, B. S. Shenoy, and K. Chethan, "Review on carbon fiber reinforced polymer (CFRP) and their mechanical performance," *Materials Today: Proceedings,* vol. 19, pp. 658-662, 2019.

[28] B. Wang, P. He, Y. Kang, J. Jia, X. Liu, and N. Li, "Ultrasonic testing of carbon fiber-reinforced polymer composites," *Journal of Sensors,* vol. 2022, no. 1, p. 5462237, 2022.

[29] Y. F. Khalil, "Eco-efficient lightweight carbon-fiber reinforced polymer for environmentally greener commercial aviation industry," *Sustainable Production and Consumption,* vol. 12, pp. 16-26, 2017.

[30] X. Yuan, W. Li, Z. Xiao, and Y. Zhang, "Prediction of temperature-dependent transverse strength of carbon fiber reinforced polymer composites by a modified cohesive zone model," *Composite Structures,* vol. 304, p. 116310, 2023.

[31] M. H. M. Yazik and I. Ismail, "Aerospace structures and engines from polymer composites," in *Aerospace Materials*: Elsevier, 2025, pp. 349-383.

[32] Q. Truong, *Composite architecture: building and design with carbon fiber and FRPs*. Birkhäuser, 2020.

[33] S. Goossens, "Barely visible impact damage detection in aerospace-grade carbon fibre reinforced polymer components with optical fibre sensors," Vrije Universiteit Brussel Brussels, Belgium, 2021.

[34] L. Piancastelli, "An innovative heat rejection system for high altitude unmanned aerial vehicles," *Power Engineering and Engineering Thermophysics,* vol. 2, no. 2, pp. 110-119, 2023.

Corresponding author: Juneed Yawar, Juneedyawar@nitsri.ac.in

[35] J. Apeland, D. Pavlou, and T. Hemmingsen, "State-of-technology and barriers for adoption of fuel cell powered multirotor drones," in *2020 International Conference on Unmanned Aircraft Systems (ICUAS)*, 2020: IEEE, pp. 1359-1367.

[36] G. Kannan, S. E. Grieshaber, and W. Zhao, "Thermoplastic polyesters," *Handbook of Thermoplastics,* vol. 41, p. 319, 2016.

[37] M. Z. Baltić *et al.*, "PETG as an alternative material for the production of drone spare parts," *Polymers,* vol. 16, no. 21, p. 2976, 2024.

[38] A. K. Pal, A. K. Mohanty, and M. Misra, "Additive manufacturing technology of polymeric materials for customized products: recent developments and future prospective," *RSC advances,* vol. 11, no. 58, pp. 36398-36438, 2021.

[39] J. Vallejo, E. García-Plaza, P. Núñez, J. Chacón, M. Caminero, and A. Romero, "Machinability analysis of carbon fibre reinforced PET-Glycol composites processed by additive manufacturing," *Composites Part A: Applied Science and Manufacturing,* vol. 172, p. 107561, 2023.

[40] M. Garwacki, I. Cudnik, D. Dziadowiec, P. Szymczak, and J. Andrzejewski, "The Development of Sustainable Polyethylene Terephthalate Glycol-Based (PETG) Blends for Additive Manufacturing Processing—The Use of Multilayered Foil Waste as the Blend Component," *Materials,* vol. 17, no. 5, p. 1083, 2024.

[41] R. Kumar, M. Kumar, and J. S. Chohan, "Material-specific properties and applications of additive manufacturing techniques: A comprehensive review," *Bulletin of Materials Science,* vol. 44, no. 3, p. 181, 2021.

[42] Y. Djemaoune, B. Krstic, S. Rasic, D. Radulovic, and M. Dodic, "Experimental investigation of an alternative approach to temporarily repair Nomex honeycomb sandwich structures in aerospace applications," *Proceedings of the Institution of Mechanical Engineers, Part L: Journal of Materials: Design and Applications,* vol. 237, no. 5, pp. 1215-1228, 2023.

[43] M. Daly, M. Tarfaoui, M. Chihi, and C. Bouraoui, "Dynamic analysis of 3D-printed CF-PETG composites with different infill densities," *Progress in Additive Manufacturing,* vol. 10, no. 2, pp. 1629-1657, 2025.

Corresponding author: Juneed Yawar, Juneedyawar@nitsri.ac.in

[44] J. Niemand, S. J. Mathew, and F. Gonzalez, "Design and testing of recycled 3D printed foldable unmanned aerial vehicle for remote sensing," in *2020 International Conference on Unmanned Aircraft Systems (ICUAS)*, 2020: IEEE, pp. 892-901.

[45] F. Popișter, H. Ș. Goia, and P. Ciudin, "Influence of Polymers Surface Roughness on Noise Emissions in 3D-Printed UAV Propellers," *Polymers,* vol. 17, no. 8, p. 1015, 2025.

[46] M. N. Saadawi, "Polymer-polymer composites: mechanical properties of inter-reinforced thermoplastics," 2019.

[47] C. de Carvalho Lucarelli, M. M. Oliveira, G. B. Pagoto, J. P. M. Pereira, and J. C. Carlo, "Structural and optical behavior of rapidly aged and unaged engineering-grade copolymers produced via fused deposition modeling," *Multiscale and Multidisciplinary Modeling, Experiments and Design,* vol. 8, no. 6, p. 286, 2025.

[48] P. Rantuch, "The thermal degradation of polymer materials," in *Ignition of Polymers*: Springer, 2022, pp. 1-43.

[49] J. H. S. Almeida Jr, S. Jayaprakash, K. Kolari, J. Kuva, K. Kukko, and J. Partanen, "The role of printing parameters on the short beam strength of 3D-printed continuous carbon fibre reinforced epoxy-PETG composites," *Composite Structures,* vol. 337, p. 118034, 2024.

[50] A. Mosaddek, H. K. Kommula, and F. Gonzalez, "Design and testing of a recycled 3D printed and foldable unmanned aerial vehicle for remote sensing," in *2018 International Conference on Unmanned Aircraft Systems (ICUAS)*, 2018: IEEE, pp. 1207-1216.

[51] X. Zhao *et al.*, "Accelerated ultraviolet aging behavior and numerical simulation of ramie/carbon fiber reinforced polyethylene terephthalate glycol hybrid composites," *Industrial Crops and Products,* vol. 205, p. 117531, 2023.

[52] A. Paesano, D. Cohee, and G. Palmese, "Carbon-fiber reinforced thermoplastic materials for rigidizable space systems," *Journal of Thermoplastic Composite Materials,* vol. 16, no. 2, pp. 139-170, 2003.

[53] K. S. Patel, D. B. Shah, S. J. Joshi, F. K. Aldawood, and M. Kchaou, "Effect of process parameters on the mechanical performance of FDM printed carbon fiber reinforced PETG," *Journal of Materials Research and Technology,* vol. 30, pp. 8006-8018, 2024.

[54] A. F. Kichloo, A. Raina, M. I. U. Haq, and M. S. Wani, "Impact of carbon fiber reinforcement on mechanical and tribological behavior of 3D-printed polyethylene

Corresponding author: Juneed Yawar, Juneedyawar@nitsri.ac.in

terephthalate glycol polymer composites—an experimental investigation," *Journal of Materials Engineering and Performance,* pp. 1-18, 2022.

[55] W. Wang *et al.*, "Additive manufacturing of continuous carbon fiber reinforced PETG with ultra-high interlaminar shear strength," *Journal of Materials Research and Technology,* vol. 34, pp. 2621-2632, 2025.

Corresponding author: Juneed Yawar, Juneedyawar@nitsri.ac.in